

Diffraction Shaders

The Longer Version

Jos Stam

Alias | Wavefront

Seattle, U.S.A.

jstam@aw.sgi.com

Abstract

The reflection of light from surfaces is a fundamental problem in computer graphics. Most previous reflection models have been either empirical or based on the ray theory of light. In this paper, conversely, we derive a new class of reflection models based on the wave theory modeling the effects of diffraction. Diffraction occurs when the surface detail is comparable to the wavelength of light. A good example is a compact disk. Our model properly models the subtle variation in intensity and color of the light reflected off of these surfaces. Our method generalizes most previous reflection models for metallic surfaces in computer graphics. In particular, we extend the He-Torrance model to anisotropic surfaces. This is achieved by rederiving, in a more general setting, results from surface wave physics which were taken for granted by other researchers. Specifically, our use of Fourier analysis has enabled us to tackle the difficult task of computing the reflected waves off of these surfaces. Our paper is of both theoretical and practical importance. The renderings and animations accompanying our paper clearly demonstrate the novelty of our approach.

1 Introduction

The modeling of the interaction of light with surfaces is one of the main goals of computer graphics. Over the last thirty years many reflection models have been proposed that have considerably improved the quality of computer graphics imagery. Almost all of these reflection models are either empirical or based on the ray theory of light. Surprisingly little attention has been devoted to the purely wave-like character of light. It is well known from physical optics that ray theory is only an approximation of the more fundamental wave theory. Why then has wave theory been so neglected? The main reason is that the ray theory is sufficient to visually capture the reflected field from many commonly occurring surfaces. This observation is usually true when the surface detail is much larger than the wavelength of visible light (roughly 0.4 microns (4×10^{-7} meters)). Another reason for this neglect is the common belief that models based on wave theory are computationally too expensive to be of any use in computer graphics. In this paper we challenge this point of view by introducing a new class of analytical reflection models which simulate the effects of *diffraction*.

Diffraction is a purely wave-like phenomenon which cannot be modeled using the standard ray theory of light. Diffraction occurs when the surface detail is comparable to the wavelength of light. A common example of a surface that produces visible diffraction patterns is the compact disk (CD). By rotating a CD under a steady light source, one can fully appreciate the visual complexity of diffraction. To capture these subtle changes in color and intensity requires a wave-like description of light. In this paper we derive analytical reflection models based on wave theory that capture the effects of diffraction. In addition, our model is both easy to implement as a standard “shader” and computationally efficient. The derivation which leads to our new model, however, is not simple. This is because the wave theory is mathematically much more complex than the ray theory of light.

Scanning through the computer graphics literature, we found only a few references which explicitly use the wave description of light. In 1981 Moravec proposed in solving the global illumination problem using the wave theory of light [18]. For his method to give acceptable results, both a very fine resolution (on the order of the wavelength of light) and a large ensemble of simulations (to model incoherent natural light sources) are required. This makes his approach unsuitable for practical computer graphics applications. Later in 1985, Kajiya proposed to numerically solve the Kirchhoff integral[‡] to simulate the light reflected from anisotropic surfaces [14]. His approach, although less ambitious than Moravec’s, suffers from the same limitations. In this context it would appear to be more promising to solve directly for the coherence functions associated with the waves, which are second order statistical averages of the wave fields. Some work in this area has been pursued by Tannenbaum et al. [30]. The coherence functions can also be employed to define generalized radiances [33].

A more practical use of the wave theory in computer graphics is to employ it to derive analytical reflection models. This approach, which has a long history in the applied optics literature, e.g., [3], was first seriously introduced to computer graphics by Bahar and Chakrabarti [2]. Using Bahar’s full wave theory they were able to fit analytical distributions to their computations for surfaces having a large isotropic surface roughness. The full wave theory has the advantage over the Kirchhoff theory in that it takes into account the global shape of the object. However, in practice analytical expressions are only known for simple objects such as spheres. Also the *global* shapes of surfaces in computer graphical models are usually much larger than the wavelength of light. Later in 1991, He and collaborators derived a general reflection model based on the electro-magnetic wave theory to predict the reflection of light from isotropic surfaces of any surface roughness [12]. At about the same time, a very similar model was proposed in the computer vision literature by Nayar [20]. As in Kajiya’s work, these two models are essentially based on the Kirchhoff approximation of surface reflection [3]. Subsequently He et al proposed a fast implementation of their model [13]. We also mention here that Blinn already used some asymptotic results from Beckmann’s monograph [4]. However, Blinn’s model does not account for wave-like effects.

Although the analytical models just discussed are based on wave theory, none of them is able to capture the visual complexity of the light reflected off of a compact disk, for example. The main reason is that these models assume the surface detail to be isotropic, i.e., the surface “looks the same” in every direction. Interesting diffraction phenomena, however, occur mostly when the surface detail is highly *anisotropic*, viz. non-isotropic. Figure 1 shows that this is certainly the case for the CD. Other examples include brushed metals and reflecting diffraction gratings used to create colorful patterns on various objects. In the latter case, pieces of the grating are placed in different orientations to create many colorful effects when the object is rotated. In computer

[‡]This integral will be defined more precisely below.

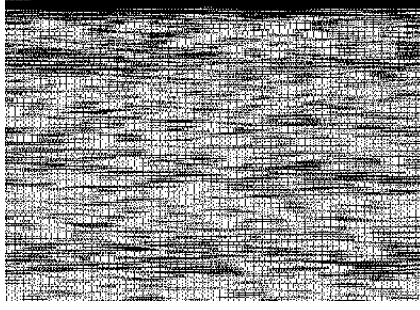


Figure 1: Close-up view of the micro-geometry of the surface of a compact disk.

graphics, both empirical and ray optics models have been proposed to model the reflection from anisotropic surfaces [22, 24, 32]. However, since these models are not based on wave theory, they failed to capture the effects of diffraction. To the best of our knowledge, reflection models that handle colorful diffraction effects have not appeared in the computer graphics literature or in any commercially available graphics software before. The phenomenon of diffraction was used, however, by Nakamae et al to model the fringes caused when viewing bright light sources through the pupil and eyelashes [19].

In this paper, we derive various analytical anisotropic reflection models using the scalar Kirchhoff wave theory and the theory of random processes. In particular, we show that the reflected intensity is equal to the spectral density of a simple function $f(x, y)$ of the (random) surface height $h(x, y)$. We show that the spectral density can be computed for a large class of surfaces not considered in previous models. We believe that our approach is novel, since the “classic” monographs on scattering from statistical surfaces do not mention such an approach [3, 21]. Although we did not consult the entire literature on this subject, we have found some related work. Sheppard and collaborators, for example, used a three-dimensional Fourier transform to compute the reflection from various surfaces [26]. However, they did not apply it to the reflection from highly anisotropic surfaces. The chapter on surface scattering in the standard *Handbook of Optics* only discusses a very simplified version of our model [6]. The simplification $f(x, y) = h(x, y)$ leads to the *first order Born approximation* which implies that the reflected field is proportional to the spectral density of the surface, not the function f used in our work. We have found, however, that the Born approximation is too coarse to visually capture colorful diffraction phenomena.

Diffraction should not be confused with the related phenomenon of *interference*. Interference produces colorful effects due to the phase differences caused by a wave traversing thin media of different indices of refraction. The most common example is that of a soap bubble. Interference effects, unlike diffraction, can be modeled using the ray theory of light alone. Smits and Meyer, for example, proposed such a model [28]. Later Gondek et al. used Monte-Carlo simulations to produce interference effects from various media such as paints [10]. This is achieved by adding a phase to every ray. The diffraction effects shown in this paper, however, could not have been generated with their model.

The remainder of this paper is organized as follows. Due to the mathematical complexity of the wave theory, some parts of our paper cannot be followed easily without some background in Fourier analysis, wave theory and the theory of random processes. We have provided two appendices that summarize the main results from these fields. A reader who is interested solely in implementing our new shaders can go directly to Section 6 where the model is stated “as is”. Section 2 summarizes the main results from wave theory which are required in this paper. Section

3 presents our derivation. Subsequently, Sections 4 and 5 present several applications of our new reflection model. Section 6 addresses implementation issues and can be read without any advanced mathematical knowledge. Section 7 discusses several results created using our new shaders. Finally, Section 8 concludes and outlines promising directions for future research.

2 Wave Theory and Computer Graphics

In this section we briefly outline some results and concepts from the wave theory necessary to understanding the derivation of our reflection model. We employ the so-called “scalar wave theory of diffraction” [5]. In this approximation the light wave is assumed to be a complex valued scalar disturbance ψ . This theory completely ignores the polarization of light, so its results are therefore restricted to unpolarized light. Fortunately, most common light sources such as the sun and light bulbs are totally unpolarized. The waves generated by these sources also have the property that they fluctuate very rapidly over time. Typical frequencies for such waves are on the order of 10^{14} s⁻¹. In practice this means that we cannot take accurate “snapshots” of a wave. Light waves are thus essentially random and only statistical averages of the wave function have any physical significance. The averaging, denoted by $\langle \cdot \rangle$, can be interpreted either as an average over a long time period or equivalently (via ergodicity) as an ensemble average. An example of a statistical quantity associated with waves is the flux of radiant energy per unit area defined by:

$$I = \langle |\psi|^2 \rangle.$$

The quantity I is important in computer graphics and is known as the *irradiance* in the radiative heat transfer literature [27].

We also assume that the waves emanating from the source are stationary. This means that the wave is a superposition of independent monochromatic waves and consequently we can restrict our analysis to a wave having a definite wavelength λ associated with it. For visible light, the wavelengths range from the ultraviolet (0.4 microns) to the infrared (1.5 microns) region. Each of these waves satisfies a Helmholtz’s wave equation:

$$\nabla^2 \psi + k^2 \psi = 0,$$

where k is the *wavenumber* associated with the wavelength

$$k = \frac{2\pi}{\lambda}.$$

The main task in the theory of diffraction is to solve this wave equation for different geometries. In our case we are interested in computing the reflected waves from various types of surfaces. More precisely, we want to compute the wave ψ_r equal to the reflection of an incoming planar monochromatic wave $\psi_i = e^{i(kz - \omega t)}$ traveling in the direction \hat{z} from a surface S . Figure 2 illustrates this situation. The equation relating the reflected field to the incoming field is known as the *Kirchhoff integral*. This equation is a formalization of Huygen’s well-known principle that states that if one knows the wavefront at a given moment, the wave at a later time can be deduced by considering each point on the first wave as the source of a new disturbance. This principle is used to relate the wave ψ_r on the surface to the field reflected off of it at a point \mathbf{r} . Mathematically, Huygen’s principle translates into a surface integral:

$$\psi_r(\mathbf{r}) = \frac{i}{2\pi} \int_S \left(\frac{\partial \psi_i}{\partial n} + \psi_i \right) \frac{e^{ik|\mathbf{r}-\mathbf{r}'|}}{|\mathbf{r}-\mathbf{r}'|} d\mathbf{r}', \quad (1)$$

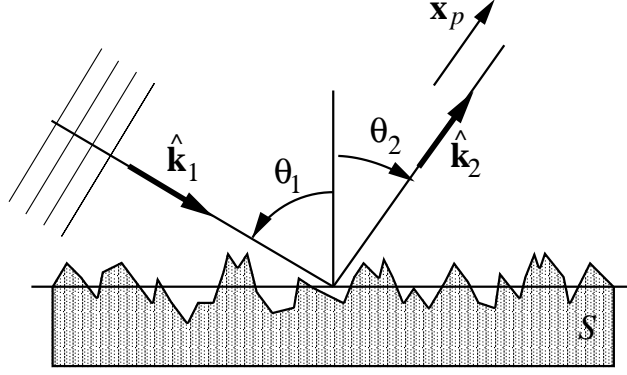


Figure 2: Basic geometry of the surface wave reflection problem.

where $\frac{\partial}{\partial n}$ denotes the derivative along the normal to the surface and r is the distance of the point \mathbf{r} on the surface to the “observation” point \mathbf{r}_p . Equation 1 shows that, in principle, once the field on the surface is known, the field everywhere else away from the surface can be computed. The field on the surface is usually related to the incoming field \mathbf{E}_i using the *tangent plane* approximation. For a planar surface, the wave theory predicts that a fraction R of the incoming light is specularly reflected. The fraction R is equal to the Fresnel factor for unpolarized light (see p. 48 of [5]). The tangent approximation states that the wave field on the surface is equal to the incoming field plus the field reflected off of the tangent plane at the surface point. Using this relation and the assumption that the “observation point” is sufficiently far removed from the surface, the Kirchhoff integral is ([3], p. 22):

$$\mathbf{E}(\mathbf{r}_p) = \frac{i}{2\pi} \int_S \frac{\partial \mathbf{E}}{\partial n} \frac{e^{ikr}}{r} dS, \quad (2)$$

where r is the distance from the center of the patch to the receiving point \mathbf{r}_p , \mathbf{n} is the normal of the surface at \mathbf{r} and the vectors

$$\mathbf{k}_1 = \frac{\mathbf{r}_p - \mathbf{r}}{|\mathbf{r}_p - \mathbf{r}|}, \quad \mathbf{k}_2 = \frac{\mathbf{r}_p - \mathbf{r}}{|\mathbf{r}_p - \mathbf{r}|} - 2(\mathbf{n} \cdot \frac{\mathbf{r}_p - \mathbf{r}}{|\mathbf{r}_p - \mathbf{r}|})\mathbf{n}.$$

The vector \mathbf{n} is equal to the unit vector pointing from the origin of the surface towards the point \mathbf{r}_p . To obtain this result it is also assumed that the Fresnel coefficient R is replaced by its average value over the normal distribution of the surface and can thus be taken out of the integral. Equation 2 is the starting point for our derivation. We will show below that it can be evaluated analytically for a large class of interesting surface profiles. Before we do so, we will also outline how the reflected wave is related to the usual reflection nomenclature used in computer graphics.

In computer graphics the reflected properties are often modeled using the bidirectional reflection distribution function (BRDF) which is defined as the ratio of the reflected radiance to the incoming irradiance. In this paper we will provide in every case the BRDF corresponding to our reflection model. In the applied optics literature, when dealing with scattered waves from a surface, one does not usually define the BRDF but rather the differential scattering cross-section defined by (e.g., [15], p. 8):

$$\frac{d\sigma}{d\Omega} = \frac{r^2}{I_i} \frac{dI_r}{d\Omega}, \quad (3)$$

The relationship between the BRDF and the scattering cross section can be shown to be equal to [31]:

[illegible]

where A is the area of the surface and θ_1 and θ_2 are the angles that the vectors \mathbf{r}_1 and \mathbf{r}_2 make with the vertical direction (see Figure 2).

3 Derivation

In this section we demonstrate that the Kirchhoff integral of Equation 2 can be computed analytically. In this paper, as in related work, we restrict ourselves to the reflection of waves from height fields. We assume that the surface is defined as an elevation over the $\langle x, y \rangle$ plane. Each surface point is then parameterized by the equation

[illegible]

where \mathbb{H} is a (random) function. The normal to the surface at each point then admits an analytical expression in terms of the partial derivatives $\partial_x \mathbb{H}$ and $\partial_y \mathbb{H}$ of the height function:

[illegible]

Introducing the notation $\mathbf{z} = \|\mathbf{z}_1, \mathbf{z}_2, \mathbf{z}_3\|$, it then follows directly that the integral in Equation 2 acquires the following form:

[illegible]

The integrand can be further simplified by noting that:

[illegible]

where

(7)

We now use the common assumption (e.g., [3, 12]) that the integration can be extended over the entire plane. This assumption is usually justified on the grounds that the surface detail is much smaller than the distances over which the surface is viewed. In doing so we observe that the integral of Eq. 6 is now a two-dimensional Fourier transform:

[illegible]

This important observation can be implemented. Let $\mathbb{F}\{\omega\}$, $\mathbb{F}\{\omega\}$ be the Fourier transform of the function \mathbb{f} . We observe from Appendix C that differentiation with respect to \mathbb{x} (resp. \mathbb{y}) in the Fourier domain is equivalent to a multiplication of the Fourier transform by $-\mathbb{i}\omega$ (resp. $-\mathbb{i}\omega$). This leads to the simple relationship

Figure 1: Schematic representation of the experimental design. The diagram illustrates the sequence of events in the experiment. It starts with a 'Stimulus' (a word 'M') and a 'Response' (a key 'M'). The response is then compared to the correct answer. If the response is correct, a green light is shown. If the response is incorrect, a red light is shown. The process then repeats for the next stimulus. The diagram is divided into two main sections: 'Stimulus' and 'Response', with a 'Feedback' section in between. The 'Stimulus' section shows a word 'M' and a key 'M'. The 'Response' section shows a key 'M' and a key 'N'. The 'Feedback' section shows a green light and a red light. The diagram is labeled 'Figure 1' and 'Schematic representation of the experimental design'.

We have thus related the integral of Equation 2 directly to the Fourier transform of the function \mathcal{H} . Now, since

$$\mathcal{H}(\mathbf{r}) = \int_{-\infty}^{\infty} \mathcal{H}(\mathbf{r}) \delta(\mathbf{r} - \mathbf{r}') d\mathbf{r}',$$

the scattered wave of Eq. 2 is equal to

$$\mathcal{H}(\mathbf{r}) = \frac{\int_{-\infty}^{\infty} \mathcal{H}(\mathbf{r}) \delta(\mathbf{r} - \mathbf{r}') d\mathbf{r}'}{\int_{-\infty}^{\infty} \delta(\mathbf{r} - \mathbf{r}') d\mathbf{r}'} \quad (8)$$

This result shows that the scattered wave field is proportional to the Fourier transform of a simple function of the surface height. Consequently, from Equations 3 and 4 of the previous section, it follows that the BRDF of the surface is

$$\mathcal{H}(\mathbf{r}) = \frac{\int_{-\infty}^{\infty} \mathcal{H}(\mathbf{r}) \delta(\mathbf{r} - \mathbf{r}') d\mathbf{r}'}{\int_{-\infty}^{\infty} \delta(\mathbf{r} - \mathbf{r}') d\mathbf{r}'} \quad (9)$$

where

$$\mathcal{H}(\mathbf{r}) = \frac{\int_{-\infty}^{\infty} \mathcal{H}(\mathbf{r}) \delta(\mathbf{r} - \mathbf{r}') d\mathbf{r}'}{\int_{-\infty}^{\infty} \delta(\mathbf{r} - \mathbf{r}') d\mathbf{r}'} \quad (10)$$

This result and the derivation that leads to it are remarkably simple when compared to derivations that do not employ the Fourier transform, e.g., [3]. More importantly, this treatment is more general, since we have not made any assumptions regarding the function \mathcal{H} yet.

We now specialize our results for a homogeneous random function ([23] and Appendix D). Homogeneity is a natural assumption since we are interested in the bulk reflection from a large portion of the surface having a certain profile. For example, the portion of the CD depicted in Figure 1 could have been taken from any part of the CD. However, and this is important, we do not assume that the surface is isotropic. This is mainly where we depart from previous wave physics models in computer graphics. Referring again to Fig. 1 we observe that the CD is clearly not isotropic.

From the definition of the function \mathcal{H} (Eq. 7) it follows immediately that this function is also homogeneous. In particular, its correlation function depends only on the separation between two locations:

$$\mathcal{H}(\mathbf{r}, \mathbf{r}') = \mathcal{H}(\mathbf{r} - \mathbf{r}', \mathbf{r}) = \mathcal{H}(\mathbf{r} - \mathbf{r}', \mathbf{r}'),$$

independently of the location \mathbf{r} . The Fourier transform of the correlation function is known as the *spectral density* ([23], p. 338):

$$\mathcal{H}(\mathbf{r}, \mathbf{r}') = \int_{-\infty}^{\infty} \mathcal{H}(\mathbf{r}, \mathbf{r}') \delta(\mathbf{r} - \mathbf{r}') d\mathbf{r} = \int_{-\infty}^{\infty} \mathcal{H}(\mathbf{r}, \mathbf{r}') \delta(\mathbf{r} - \mathbf{r}') d\mathbf{r}.$$

The spectral density is a non-negative function which gives the relative contribution of each wavenumber \mathbf{k} to the entire energy. We now show that the average in Eq. 9 is directly related to the spectral density. Indeed,

$$\mathcal{H}(\mathbf{r}, \mathbf{r}') = \int_{-\infty}^{\infty} \mathcal{H}(\mathbf{r}, \mathbf{r}') \delta(\mathbf{r} - \mathbf{r}') d\mathbf{r} = \int_{-\infty}^{\infty} \mathcal{H}(\mathbf{r}, \mathbf{r}') \delta(\mathbf{r} - \mathbf{r}') d\mathbf{r}.$$

With the change of variable $\mathbf{r} = \mathbf{r} + \mathbf{r}'$, this integral becomes

$$\mathcal{H}(\mathbf{r}, \mathbf{r}') = \int_{-\infty}^{\infty} \mathcal{H}(\mathbf{r}, \mathbf{r}') \delta(\mathbf{r} - \mathbf{r}') d\mathbf{r} = \int_{-\infty}^{\infty} \mathcal{H}(\mathbf{r}, \mathbf{r}') \delta(\mathbf{r} - \mathbf{r}') d\mathbf{r}.$$

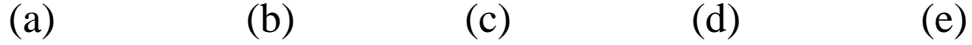


Figure 3: Effect of the correlation function on the appearance of a random surface. The pictures at the top show plots of different correlation functions with a realization of the corresponding random surface below. The surface types are: (a) isotropic Gaussian, (b) anisotropic Gaussian, (c) isotropic fractal, (d) anisotropic fractal and (e) another type of fractal anisotropy. See the text for the exact definitions of these correlation functions.

where $\delta(\mathbf{r})$ is the two-dimensional Dirac delta function. Consequently, the average in Eq. 9 is a function of the spectral density of the function η :

$$\frac{1}{A} \int_A \langle |\eta(\mathbf{r})|^2 \rangle d\mathbf{r} = \int d\mathbf{r} \langle |\eta(\mathbf{r})|^2 \rangle \delta(\mathbf{r}) = \int d\mathbf{r} \langle |\eta(\mathbf{r})|^2 \rangle \delta(\mathbf{r}).$$

Substituting this result back into Eq. 9 we get:

$$\langle |\eta(\mathbf{r})|^2 \rangle = \frac{1}{A} \int d\mathbf{r} \langle |\eta(\mathbf{r})|^2 \rangle \delta(\mathbf{r}) = \int d\mathbf{r} \langle |\eta(\mathbf{r})|^2 \rangle \delta(\mathbf{r}), \quad (11)$$

where we have used the fact that $\langle |\eta(\mathbf{r})|^2 \rangle = \langle |\eta(\mathbf{r})|^2 \rangle \delta(\mathbf{r})$ [34]. Eq. 11 is the main theoretical result of this paper. It shows that the reflection from a random surface is proportional to the spectral density of the random function $\eta(\mathbf{r})$. In the next two sections we apply this result to the derivation of reflection models for various types of surfaces.

4 Diffraction From Anisotropic Rough Surfaces

4.1 General Case

Every surface shown in Figure 3 is a realization of a *Gaussian random process*. These processes have the property that they are entirely defined by their corresponding correlation function depicted in the upper part of Figure 3. From the figure it is clear that the correlation function determines the general appearance of the random surface. Radially symmetrical correlation functions correspond to isotropic surfaces, c.f., surfaces (a) and (c), while the behavior of the correlation function at the origin also determines how smooth the surfaces are. Consequently, surfaces (a) and (b) are smooth,

while surfaces (c), (d) and (e) have a fractal appearance. In this section we further clarify the fact that the reflection from these surfaces is intimately related to the correlation function. Gaussian random processes have the nice property that their characteristic functions admit analytical expressions (see Appendix D). These functions are exactly what we require in order to compute the spectral density \mathcal{S}_{η} and the variance $\langle \eta^2 \rangle$ appearing in Equation 11. Indeed, for Gaussian random processes these quantities are related to their surface height counterparts as follows. Firstly, we have the following identities ([23], p. 255):

$$\langle \eta^2 \rangle = \int_{-\infty}^{\infty} \mathcal{S}_{\eta}(\mathbf{k}) d\mathbf{k} \quad (12)$$

$$\langle \eta^2 \rangle = \int_{-\infty}^{\infty} \langle \eta(\mathbf{r}) \eta(\mathbf{r} + \mathbf{r}') \rangle d\mathbf{r} \quad (13)$$

where

$$\langle \eta^2 \rangle = \sigma_{\eta}^2$$

and σ_{η} is the standard deviation of the height fluctuations. Secondly, the spectral density \mathcal{S}_{η} is the Fourier transform of the correlation function $\langle \eta(\mathbf{r}) \eta(\mathbf{r} + \mathbf{r}') \rangle$ ([23], p. 338). To compute this Fourier transform analytically we use the usual expansion of the exponential function into an infinite series [3]:

$$\exp(i\mathbf{k} \cdot \mathbf{r}) = \sum_{n=0}^{\infty} \frac{(i\mathbf{k} \cdot \mathbf{r})^n}{n!} = \sum_{n=0}^{\infty} \frac{i^n}{n!} \mathbf{k} \cdot \mathbf{r}^n$$

By the linearity of the Fourier transform we then have that

$$\mathcal{S}_{\eta}(\mathbf{k}) = \int_{-\infty}^{\infty} \langle \eta(\mathbf{r}) \eta(\mathbf{r} + \mathbf{r}') \rangle \exp(i\mathbf{k} \cdot \mathbf{r}) d\mathbf{r} \quad (14)$$

This requires the computation of the Fourier transform of the surface correlation to a power η^n . We now give analytical results for the three correlation functions corresponding to the surfaces depicted in Figure 3. These surfaces are defined by the following three correlation functions:

$$\langle \eta(\mathbf{r}) \eta(\mathbf{r} + \mathbf{r}') \rangle = \frac{\sigma_{\eta}^2}{2} \left(1 - \frac{|\mathbf{r}|}{\ell_{\parallel}} - \frac{|\mathbf{r}'|}{\ell_{\perp}} \right), \quad \langle \eta(\mathbf{r}) \eta(\mathbf{r} + \mathbf{r}') \rangle = \frac{\sigma_{\eta}^2}{2} \left(1 - \frac{|\mathbf{r}|}{\ell_{\parallel}} - \frac{|\mathbf{r}'|}{\ell_{\perp}} \right), \quad \langle \eta(\mathbf{r}) \eta(\mathbf{r} + \mathbf{r}') \rangle = \frac{\sigma_{\eta}^2}{2} \left(1 - \frac{|\mathbf{r}|}{\ell_{\parallel}} - \frac{|\mathbf{r}'|}{\ell_{\perp}} \right).$$

In all three cases, the *correlation lengths* ℓ_{\parallel} and ℓ_{\perp} control the anisotropy of the surface. Figures 3.(a) and (b) both correspond to the correlation function $\langle \eta(\mathbf{r}) \eta(\mathbf{r} + \mathbf{r}') \rangle$. This function is infinitely smooth at the origin, which accounts for the smoothness of the corresponding surfaces. In Figure 3.(a) $\ell_{\parallel} = \ell_{\perp}$ and the surfaces are isotropic. Most previous wave-based models considered only the isotropic case. Figures 3.(c) and (d) correspond to the correlation function $\langle \eta(\mathbf{r}) \eta(\mathbf{r} + \mathbf{r}') \rangle$. The corresponding surfaces have a fractal appearance. They are thus good models for very rough materials. In the result section we will see that these surfaces give rise to reflection patterns which are visually different from the smooth case. The correlation function $\langle \eta(\mathbf{r}) \eta(\mathbf{r} + \mathbf{r}') \rangle$ is anisotropic even when $\ell_{\parallel} = \ell_{\perp}$. A corresponding realization is depicted in Figure 3.(e).

For each correlation function, we can compute its Fourier transforms to a power η^n analytically. For $\langle \eta^2 \rangle$, $\langle \eta^4 \rangle$ and $\langle \eta^6 \rangle$ they are equal to [1]:

$$\langle \eta^2 \rangle = \int_{-\infty}^{\infty} \mathcal{S}_{\eta}(\mathbf{k}) d\mathbf{k}, \quad \langle \eta^4 \rangle = \int_{-\infty}^{\infty} \mathcal{S}_{\eta}(\mathbf{k}) \mathcal{S}_{\eta}(\mathbf{k}') d\mathbf{k} d\mathbf{k}', \quad \langle \eta^6 \rangle = \int_{-\infty}^{\infty} \mathcal{S}_{\eta}(\mathbf{k}) \mathcal{S}_{\eta}(\mathbf{k}') \mathcal{S}_{\eta}(\mathbf{k}'') d\mathbf{k} d\mathbf{k}' d\mathbf{k}'', \quad (15)$$

[illegible]

Keywords: child sexual abuse; disclosure; social support; coping strategies

1. $\frac{1}{2} \times \frac{1}{2} = \frac{1}{4}$

— 1 —

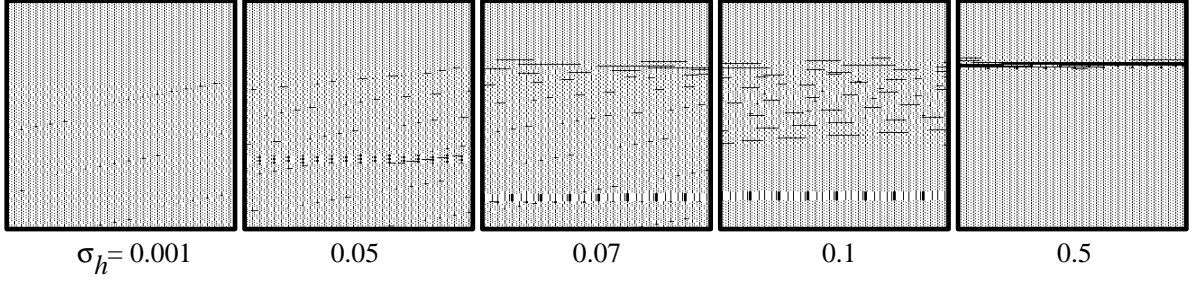


Figure 4: Plots of the BRDF for σ_h ranging from the infrared (10^{-4}) to the ultraviolet region (10^{-1}). The reflection is in the specular direction: $\theta_r = \theta_i = \theta_h$. The plots show the effect of the standard deviation σ_h on the color of the reflection. For low deviations the reflection is bluish, while for higher roughness it tends to flatten out. The dashed line is the geometrical optics approximation.

from the wave theory but rather from the ray theory of light. For large σ_h , the Fourier integral only depends on the behavior of the function σ_h^2 near the origin (see [3, 2] for details):

$$\sigma_h^2 \approx \frac{1}{2\pi} \int_{-\infty}^{\infty} \sigma_h^2(\mathbf{u}) e^{-i\mathbf{u} \cdot \mathbf{u}_0} d\mathbf{u}.$$

The Fourier transform of this function can be computed analytically and is equal to:

$$\sigma_h^2(\mathbf{u}) = \frac{1}{2\pi} \int_{-\infty}^{\infty} \sigma_h^2(\mathbf{u}') e^{-i\mathbf{u}' \cdot \mathbf{u}} d\mathbf{u}' = \frac{1}{2\pi} \int_{-\infty}^{\infty} \sigma_h^2(\mathbf{u}') e^{-i\mathbf{u}' \cdot \mathbf{u}} d\mathbf{u}'.$$

The BRDF in this case is equal to ($\theta_r = \theta_i = \theta_h$):

$$\sigma_h^2(\mathbf{u}) = \frac{1}{2\pi} \int_{-\infty}^{\infty} \sigma_h^2(\mathbf{u}') e^{-i\mathbf{u}' \cdot \mathbf{u}} d\mathbf{u}' = \frac{1}{2\pi} \int_{-\infty}^{\infty} \sigma_h^2(\mathbf{u}') e^{-i\mathbf{u}' \cdot \mathbf{u}} d\mathbf{u}', \quad (17)$$

where

$$\sigma_h^2(\mathbf{u}) = \frac{1}{2\pi} \int_{-\infty}^{\infty} \sigma_h^2(\mathbf{u}') e^{-i\mathbf{u}' \cdot \mathbf{u}} d\mathbf{u}' = \frac{1}{2\pi} \int_{-\infty}^{\infty} \sigma_h^2(\mathbf{u}') e^{-i\mathbf{u}' \cdot \mathbf{u}} d\mathbf{u}'.$$

This distribution is a generalization of the isotropic distributions found in Blinn and Cook-Torrance where there is only one roughness parameter “ σ_h ”. In fact, our model closely resembles Ward’s anisotropic reflection model [32]. As in the Cook-Torrance model, $\sigma_h^2(\mathbf{u})$ is only dependent on the wavelength of light through the Fresnel factor F , as there is no other explicit dependence on wavelength: λ does not explicitly appear in the distribution.

Isotropic Distributions

The He-Torrance [12] and the Nayar [20] reflection models are obtained when our model is restricted to the class of isotropic surfaces corresponding to Figure 3.(a). Using our result for the correlation function σ_h^2 with $\sigma_h = \sigma_h$, we essentially recover both of these models. It is worth noting that one of the versions of the He-Torrance model handles polarization effects while our model doesn’t. This is because they used the vector valued version of the Kirchhoff integral. However, in practice it seems He-Torrance have only used their unpolarized version to create the pictures accompanying their paper. The dependence on wavelength (as in our model) is a function of the

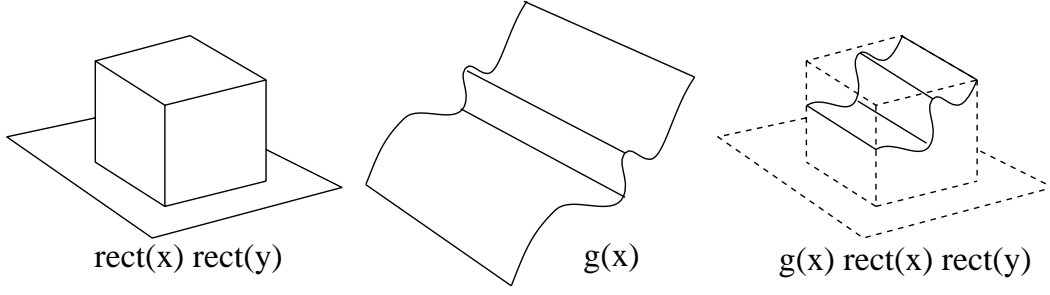


Figure 5: Each bump is defined as the multiplication of a function $g(x, y)$ with the product of box-like functions.

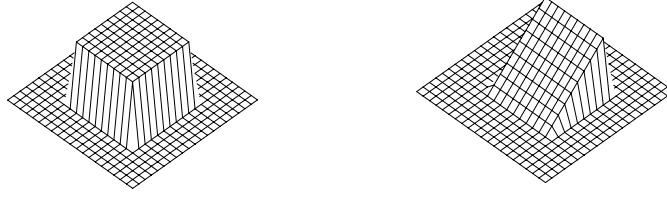


Figure 6: Two different bump functions: (1) constant, (2) linear in one coordinate.

Fresnel factor R and the function $g(x, y)$. In Figure 4 we illustrate the dependence of this function on wavenumber k for different surface deviations σ . The reflection goes from a k^2 dependence to a flat spectrum. Notice that in the midrange we actually get a small yellowish hue. The figure also demonstrates that for $\sigma \ll \lambda$ the geometrical optics model, shown as a dashed line, is a very good approximation. In practice we have found that whenever $\sigma \ll \lambda$ the pictures generated with the geometrical optics approximation are visually indistinguishable from pictures generated using the exact model.

5 Diffraction from Periodic-like Surfaces

We now turn to an application that most clearly demonstrates the power of our new reflection model.

Many surfaces have a micro-structure that is made out of similar “bumps”. A good example is a compact disk which has small bumps that encode the information distributed over each “track”. Fig. 1 is a magnified view of the actual surface of a compact disk. Notice in particular that the distribution of bumps is random along each track but that the tracks are evenly spaced. In this section we derive general formulae for certain shapes of bumps, and then specialize the results for a CD-shader.

We assume that the surface is given by a superposition of bumps:

$$z(x, y) = \sum_{i,j} g(x, y) \cdot \text{rect}\left(\frac{x - x_{ij}}{\Delta x}\right) \cdot \text{rect}\left(\frac{y - y_{ij}}{\Delta y}\right), \quad (18)$$

¹⁰ In reality there is only one long spiral-like track on a compact disk. In practice, this long track can be approximated by many concentric tracks of decreasing radii.

symbol	description	size
h	height of a bump	0.15 μm
w	width of a bump	0.5 μm
l	length of a bump	1 μm
s	separation between the tracks	2.5 μm
ρ	density of bumps on each track	0.5 μm^{-1}

Table 1: Typical dimensions of a compact disk.

where the locations $\{x_n, y_n\}$ are assumed to be either regularly spaced or randomly (Poisson) distributed. To handle the two cases simultaneously, we assume that x_n is evenly spaced and that y_n is Poisson distributed. Extensions to the case where both locations are evenly spaced or where both are Poisson distributed should be obvious from our results. Let s be the constant spacing between the x_n -locations: $x_n = ns$. The random Poisson distribution of the locations y_n is entirely specified by a density ρ of bumps per unit length. The function $\delta(x, y)$ appearing in Eq. 18 is a “bump function”: a function with (small) finite support. We will assume that the bump function has the following simple form:

$$\delta(x, y) = h \cdot \text{rect}\left(\frac{x}{w}\right) \cdot \text{rect}\left(\frac{y}{l}\right), \quad (19)$$

where w , l and h define the width, length and height of each bump respectively (rect is the “rectangle” function of support $[-1, 1]$):

$$\text{rect}(x) = \begin{cases} 1 & |x| \leq 1 \\ 0 & \text{otherwise} \end{cases}.$$

Figure 5 illustrates our definition of a bump. Our derivation is valid for arbitrary δ , however, we provide an analytical expression only for the following two functions:

$$\delta(x, y) = h \cdot \text{rect}\left(\frac{x}{w}\right) \cdot \text{rect}\left(\frac{y}{l}\right) \quad \text{and} \quad \delta(x, y) = h \cdot \text{rect}\left(\frac{x}{w}\right) \cdot \delta(y). \quad (20)$$

The bumps corresponding to these functions are depicted in Figure 6. The function δ^{rect} is a good approximation of the bumps found on a CD and the function δ^{delta} can be used to model diffraction gratings.

The function $\delta(x, y)$ defined by Eq. 7 in our case is equal to:

$$\delta(x, y) = h \cdot \sum_n \text{rect}\left(\frac{x - ns}{w}\right) \cdot \text{rect}\left(\frac{y - y_n}{l}\right) + \delta(x, 0), \quad (21)$$

where

$$\delta(x, y) = \begin{cases} 1 & |x| \leq 1 \\ 0 & \text{otherwise} \end{cases}.$$

and $\delta(x, 0) = \delta(x)$. The constant term “ δ ” accounts for the space between the bumps and adds a delta spike in the specular direction. To simplify the following derivation we will drop this constant term. This is amply justified by the fact that we are mainly interested in the diffraction caused by the bumps (see also p. 353 of [17] for a related argument).

A simple computation shows that the Fourier transform of the function $\sum_{n \in \mathbb{Z}} \delta(x - n)$ is equal to $\sum_{k \in \mathbb{Z}} \delta(k)$ (remembering that we are dropping the constant term “1” in Eq. 21)

$$\sum_{n \in \mathbb{Z}} \delta(x - n) \xrightarrow{\text{FT}} \sum_{k \in \mathbb{Z}} \delta(k),$$

where $\sum_{k \in \mathbb{Z}} \delta(k)$ is the Fourier transform of $\sum_{n \in \mathbb{Z}} \delta(x - n)$ and

$$\sum_{n \in \mathbb{Z}} \delta(x - n) \xrightarrow{\text{FT}} \sum_{k \in \mathbb{Z}} \delta(k) \quad (22)$$

To compute the spectral density of Equation 11 we note that:

$$\sum_{n \in \mathbb{Z}} \delta(x - n) \xrightarrow{\text{FT}} \sum_{k \in \mathbb{Z}} \delta(k) \quad \text{and} \quad \sum_{n \in \mathbb{Z}} \delta(x - n) \xrightarrow{\text{FT}} \sum_{k \in \mathbb{Z}} \delta(k).$$

The spectral density and the average of the sum of random Poisson distributed locations are both equal to the density $\sum_{n \in \mathbb{Z}} \delta(x - n)$ (see [23] p. 561):

$$\sum_{n \in \mathbb{Z}} \delta(x - n) \xrightarrow{\text{FT}} \sum_{k \in \mathbb{Z}} \delta(k) \quad \text{and} \quad \sum_{n \in \mathbb{Z}} \delta(x - n) \xrightarrow{\text{FT}} \sum_{k \in \mathbb{Z}} \delta(k).$$

The sum of evenly spaced location $\sum_{n \in \mathbb{Z}} \delta(x - n)$ is a bit harder to deal with. First we need the following two results from the theory of distributions (see pp. 54-55 of reference [34]):

$$\sum_{n \in \mathbb{Z}} \delta(x - n) \xrightarrow{\text{FT}} \sum_{k \in \mathbb{Z}} \delta(k) \quad \text{and} \quad \sum_{n \in \mathbb{Z}} \delta(x - n) \xrightarrow{\text{FT}} \sum_{k \in \mathbb{Z}} \delta(k),$$

where a and b are real numbers. The first of these two equalities is known as “Poisson’s summation formula”. Using these results we can express the sum $\sum_{n \in \mathbb{Z}} \delta(x - n)$ in terms of delta distributions only:

$$\sum_{n \in \mathbb{Z}} \delta(x - n) \xrightarrow{\text{FT}} \sum_{k \in \mathbb{Z}} \delta(k) \quad \text{and} \quad \sum_{n \in \mathbb{Z}} \delta(x - n) \xrightarrow{\text{FT}} \sum_{k \in \mathbb{Z}} \delta(k).$$

The square of this function is equal to

$$\left(\sum_{n \in \mathbb{Z}} \delta(x - n) \right)^2 \xrightarrow{\text{FT}} \sum_{k \in \mathbb{Z}} \delta(k) \quad \text{and} \quad \left(\sum_{n \in \mathbb{Z}} \delta(x - n) \right)^2 \xrightarrow{\text{FT}} \sum_{k \in \mathbb{Z}} \delta(k).$$

We can now compute the spectral density $\sum_{k \in \mathbb{Z}} \delta(k)$ by putting all these computations together:

$$\sum_{k \in \mathbb{Z}} \delta(k) \xrightarrow{\text{FT}} \sum_{n \in \mathbb{Z}} \delta(x - n) \quad (23)$$

where

$$\sum_{k \in \mathbb{Z}} \delta(k) \xrightarrow{\text{FT}} \sum_{n \in \mathbb{Z}} \delta(x - n) \quad \text{and} \quad \sum_{k \in \mathbb{Z}} \delta(k) \xrightarrow{\text{FT}} \sum_{n \in \mathbb{Z}} \delta(x - n).$$

and we made use of the following identities

$$\sum_{k \in \mathbb{Z}} \delta(k) \xrightarrow{\text{FT}} \sum_{n \in \mathbb{Z}} \delta(x - n) \quad \text{and} \quad \sum_{k \in \mathbb{Z}} \delta(k) \xrightarrow{\text{FT}} \sum_{n \in \mathbb{Z}} \delta(x - n).$$

The function \mathcal{F} can be computed analytically for each of the simple bumps depicted in Figure 6 and defined in Equation 20:

$$\begin{aligned} \mathcal{F}_{\text{rect}}(\mathbf{u}, \mathbf{v}) &= \frac{1}{\text{area}} \int_{\text{rect}} \exp(i\mathbf{u} \cdot \mathbf{x} + i\mathbf{v} \cdot \mathbf{y}) d\mathbf{x} d\mathbf{y}, \\ \mathcal{F}_{\text{tri}}(\mathbf{u}, \mathbf{v}) &= \frac{1}{\text{area}} \int_{\text{tri}} \exp(i\mathbf{u} \cdot \mathbf{x} + i\mathbf{v} \cdot \mathbf{y}) d\mathbf{x} d\mathbf{y}, \end{aligned}$$

where the “sinc” function is equal to

$$\text{sinc}(x) = \frac{\sin(x)}{x}.$$

Their squares are equal to

$$|\mathcal{F}_{\text{rect}}(\mathbf{u}, \mathbf{v})|^2 = \frac{1}{\text{area}^2} \int_{\text{rect}} \int_{\text{rect}} \exp(i\mathbf{u} \cdot (\mathbf{x} - \mathbf{x}') + i\mathbf{v} \cdot (\mathbf{y} - \mathbf{y}')) d\mathbf{x} d\mathbf{y} d\mathbf{x}' d\mathbf{y}', \quad (24)$$

$$|\mathcal{F}_{\text{tri}}(\mathbf{u}, \mathbf{v})|^2 = \frac{1}{\text{area}^2} \int_{\text{tri}} \int_{\text{tri}} \exp(i\mathbf{u} \cdot (\mathbf{x} - \mathbf{x}') + i\mathbf{v} \cdot (\mathbf{y} - \mathbf{y}')) d\mathbf{x} d\mathbf{y} d\mathbf{x}' d\mathbf{y}'. \quad (25)$$

Putting all these pieces together we get the following expression for the BRDF:

$$f_r(\mathbf{u}, \mathbf{v}) = \frac{1}{\text{area}} \int_{\text{rect}} \exp(i\mathbf{u} \cdot \mathbf{x} + i\mathbf{v} \cdot \mathbf{y}) \left(|\mathcal{F}_{\text{rect}}(\mathbf{u}, \mathbf{v})|^2 + |\mathcal{F}_{\text{tri}}(\mathbf{u}, \mathbf{v})|^2 \right) d\mathbf{x} d\mathbf{y}. \quad (26)$$

Had we assumed that the locations \mathbf{x}_i were also Poisson distributed with density $\rho_{\mathbf{x}}$, then the spectral density would have been equal to:

$$\mathcal{F}_{\text{rect}}(\mathbf{u}, \mathbf{v}) = \frac{1}{\text{area}} \int_{\text{rect}} \exp(i\mathbf{u} \cdot \mathbf{x} + i\mathbf{v} \cdot \mathbf{y}) d\mathbf{x} d\mathbf{y},$$

a much simpler expression than when a regular spacing is present.

6 Implementation

We have implemented our reflection models as various shaders in our MAYA animation system. Any model created in that package can be rendered using our new shaders. The fact that our shaders have been included in a commercial product should be a sufficient proof of their practicality.

As in [14], we model the anisotropy of the surface by assigning an orthonormal frame at each point of the surface. In the case of a parametric surface, the most natural choice for this frame is to take the normal and the two vectors tangent to the iso-parameter lines. We have also added an additional rotation angle to the frame around the normal. When this angle is texture mapped, it allows us to create effects such as brushed metal (Fig. 9.(a)).

The general form of our shader is

$$f_r(\mathbf{u}, \mathbf{v}) = \frac{1}{\text{area}} \int_{\text{rect}} \exp(i\mathbf{u} \cdot \mathbf{x} + i\mathbf{v} \cdot \mathbf{y}) \left(F(\theta) S(\mathbf{u}, \mathbf{v}) G(\mathbf{u}, \mathbf{v}) \text{Env}(\mathbf{u}, \mathbf{v}) \right) d\mathbf{x} d\mathbf{y},$$

where F is the Fresnel factor [7], S is a shadowing function [12], G is a geometrical factor defined by Equation 10 in Section 3 and Env is a distribution function that is related to the micro-geometry of the surface. The function “Env” returns the color in the mirror direction of \mathbf{u} from an environment map and the factor S accounts for how much the surface reflects direct illumination. The vector $\mathbf{u} = \frac{\mathbf{u}_x}{\|\mathbf{u}\|}, \mathbf{v} = \frac{\mathbf{v}_y}{\|\mathbf{v}\|}$ is the angle midway between $-\mathbf{u}$ and \mathbf{u} . The Fresnel factor is evaluated at the angle $\theta = \arccos(\mathbf{u} \cdot \mathbf{n})$.

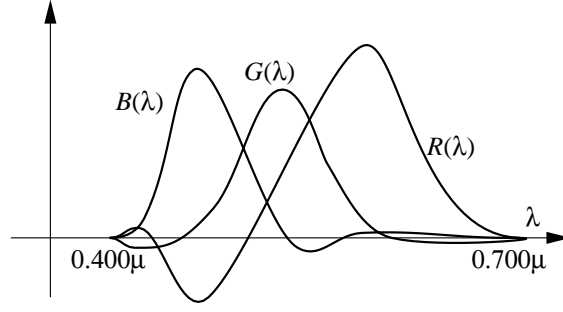


Figure 7: Spectral response curves for red, green and blue.

that the direction $\hat{\omega}_r$ makes with the vector $\hat{\omega}_i$. We do not use the He-Torrance shadowing function since it is restricted to isotropic surfaces. Instead, we employ a model introduced by Sancer [25]. For convenience, we have included this model in Appendix A. The shadowing function accounts for masking at glancing angles. The distribution \mathcal{D} is the most important component of our model and is now described in some more detail.

In the previous sections we have derived distribution functions for both the random surfaces depicted in Figure 3 and for periodic-like profiles such as the one in Figure 1. When the surface is random, the distribution is defined by three parameters σ , ℓ_x and ℓ_y . The variance σ^2 models the average height fluctuations of the surface and the parameters ℓ_x and ℓ_y model the amount of correlation of the micro-surface in the directions of the local frame. See Section 3 for further details on these quantities. When $\ell_x = \ell_y$, the surface is isotropic. In the most general case, the distribution \mathcal{D} is computed by the infinite sum appearing in Equation 16. In Appendix B, we provide a stable implementation of this sum. Alternatively the infinite sum can be approximated with spline functions as in [13]. As pointed out in the previous section, the sum is very well approximated by the geometrical optics approximation of Equation 17, when $\sigma \gg \ell_x, \ell_y$ is large. The factor “ σ ” is equal to $\sqrt{\ell_x^2 + \ell_y^2}$. The smoother the surface, the more indirect illumination is directly reflected off of it.

The implementation for periodic-like profiles giving rise to colorful diffraction patterns is different. When evaluating the distribution \mathcal{D} , the values θ and ϕ (and \mathbf{m}) are determined by the incoming and outgoing angles. The incoming light is usually assumed to be an incoherent sum of many monochromatic waves whose number is proportional to the distribution $\mathcal{D}(\lambda)$ of the light source. To determine the intensity and the color of the light that is reflected in the outgoing direction, we first compute the wavelengths λ_m for which $\mathcal{D}(\lambda_m)$ is non zero and for which the delta spikes in Eq. 23 are non-zero. This only occurs when:

$$\frac{\sin \theta \cos \phi}{\lambda_m} = \frac{m_x}{\ell_x} + \frac{m_y}{\ell_y},$$

where $\mathbf{m} \in \mathbb{Z}^2$. When $\theta = 0$, all wavelengths contribute intensities in the specular direction $\theta = 0$. In general, visible light is comprised only of waves with wavelengths between $\lambda_{\min} \approx 0.4 \mu\text{m}$ and $\lambda_{\max} \approx 0.7 \mu\text{m}$. This means that the indices \mathbf{m} are constrained to lie in the range:

$$\left\lceil \frac{\sin \theta \cos \phi}{\lambda_{\max}} \right\rceil \leq \frac{m_x}{\ell_x} + \frac{m_y}{\ell_y} \leq \left\lfloor \frac{\sin \theta \cos \phi}{\lambda_{\min}} \right\rfloor$$

if $\ell_x, \ell_y > 0$ and

when $\lambda = \lambda_0$. Once these wavelengths are determined the red, green and blue components of the distribution $D(\lambda)$ are computed as follows

$$D(\lambda) = \frac{1}{\sum_{i=1}^3 D_i(\lambda)} \left(D_1(\lambda) \begin{bmatrix} R \\ G \\ B \end{bmatrix}_1 + D_2(\lambda) \begin{bmatrix} R \\ G \\ B \end{bmatrix}_2 + D_3(\lambda) \begin{bmatrix} R \\ G \\ B \end{bmatrix}_3 \right),$$

where $\begin{bmatrix} R \\ G \\ B \end{bmatrix}_i$ is a function that for each wavelength returns the corresponding color. This function can be built using the spectral response curves shown in Figure 7, for example. See Equation 26 for a definition of the function $\begin{bmatrix} R \\ G \\ B \end{bmatrix}_i$.

7 Results

Once the shaders were implemented in MAYA, it was an easy task to generate results demonstrating the power of our new shading model. In Fig. 8 we show the effect of some of the parameters of our model on the appearance of the surfaces. In each rendering we chose to have a spectrally flat Fresnel factor to demonstrate the dependence of the distribution on wavelength. For the Gaussian correlations the reflection is more bluish for small roughness and becomes whiter for larger roughness, in accordance with the analysis of Section 4.2. The reflection from fractal surfaces is quite interesting: bluish for small roughness, then yellowish for intermediate roughness and finally white for large roughness. The third row of spheres exhibits the effect of the separation and twist angle parameters of our diffraction shader. We used a different texture map for the twist angle of each one of the three “diffraction cones” at the bottom of Fig. 8.

Fig. 9 shows several renderings created in this manner. In each case we have texture mapped the directions of anisotropy to add more interesting visual detail. Fig. 9.(a) demonstrates that this can be employed to create a “brushed metal” look. In Fig. 9.(b) we textured both the roughness and the degree of anisotropy of the surface. Fig. 9.(c) is a picture of a CD illuminated by a directional light source. Notice that all the highlights appear automatically in the correct places when the data from Table 1 is used. Fig. 9.(d) is an example of the use of our diffraction grating model. Notice all the subtle coloring effects that result (especially when viewing the corresponding animation). These colorful effects would be hard to model by trial and error without properly modeling the wave properties of light.

The effects of the anisotropy and of diffraction are most pronounced in an animation when moving either the object or the light sources. For this reason we have included some animations on the CDROM proceedings.

8 Conclusions

In this paper we have proposed a new class of reflection models that take into account the wave-like properties of light. For the first time in computer graphics, we have derived reflection models that properly simulate the effects of diffraction. We have shown that our models can be easily implemented as standard shaders in our MAYA animation software. Our derivations, while mathematically involved, are simpler and more general than previously published results in this area. In particular, our use of the Fourier transform has proven to be a very powerful tool in deriving new reflection models.

In future work, we hope to extend our model to an even wider class of surfaces by relaxing some of the assumptions in our model. Presently, our model only accounts for the reflection from metallic surfaces and ignores multiple-scattering. It would be interesting to derive more general models that take into account subsurface scattering by waves (Reference [11] does not use the wave theory of light). It seems unlikely that the effects of multiple scattering might be captured by an analytical model. An alternative would be to fit analytical models to either the results from a Monte-Carlo wave simulation or experimentally measured data. The latter approach seems to be the one currently pursued by the Cornell group [9].

As well, we wish to extend our work to the computation of the fluctuations of the intensity field [16]. In this manner we can compute exact texture maps for given surface profiles. We could achieve this by deriving analytical expressions for the higher order statistics of the reflected intensity field. More specifically, we hope to extend our previous work on stochastic rendering of density fields to surfaces [29].

Acknowledgments

Thanks to Duncan Brinsmead for suggesting the “twist angle”, for helping me write the MAYA plugin and for creating Figs. 9.(a) and (b). Thanks to Greg Ward for encouraging me to study the wave theory and for commenting on the first draft of this paper. Thanks also to Pamela Jackson for proofreading the paper.

References

- [1] M. Abramowitz and C. A. Stegun. *Handbook of Mathematical Functions with Formulas, Graphs, and Mathematical Tables*, 9th printing. Dover, New York, 1072.
- [2] E. Bahar and S. Chakrabarti. Full-Wave Theory Applied to Computer-Aided Graphics for 3D Objects. *IEEE Computer Graphics and Applications*, 7(7):46–60, July 1987.
- [3] P. Beckmann and A. Spizzichino. *The Scattering of Electromagnetic Waves from Rough Surfaces*. Pergamon, New York, 1963.
- [4] J. F. Blinn. Models of Light Reflection for Computer Synthesized Pictures. *ACM Computer Graphics (SIGGRAPH '77)*, 11(3):192–198, August 1977.
- [5] M. Born and E. Wolf. *Principles of Optics. Sixth (corrected) Edition*. Cambridge University Press, Cambridge, U.K., 1997.
- [6] E. L. Church and P. Z. Takacs. *Chapter 7. Surface Scattering*. In *Handbook of Optics (Second Edition). Volume I: Fundamentals, Techniques and Design*. McGraw Hill, New York, 1995.
- [7] R. L. Cook and K. E. Torrance. A Reflectance Model for Computer Graphics. *ACM Computer Graphics (SIGGRAPH '81)*, 15(3):307–316, August 1981.
- [8] H. C. Van de Hulst. *Light Scattering by Small Particles*. Dover, New York, 1981.
- [9] D. P. Greenberg et al. A Framework for Realistic Image Synthesis. In *Computer Graphics Proceedings, Annual Conference Series*, 1997, pages 477–494, August 1997.

- [10] J. S. Gondek, G. W. Meyer, and J. G. Newman. Wavelength dependent reflectance functions. In *Computer Graphics Proceedings, Annual Conference Series, 1993*, pages 213–220, 1994.
- [11] P. Hanrahan and W. Krueger. Reflection from Layered Surfaces due to Subsurface Scattering. In *Proceedings of SIGGRAPH '93*, pages 165–174. Addison-Wesley Publishing Company, August 1993.
- [12] X. D. He, K. E. Torrance, F. X. Sillion, and D. P. Greenberg. A Comprehensive Physical Model for Light Reflection. *ACM Computer Graphics (SIGGRAPH '91)*, 25(4):175–186, July 1991.
- [13] X. D. He, P. O. Heynen R. L. Phillips K. E. Torrance, D. H. Salesin, and D. P. Greenberg. A Fast and Accurate Light Reflection Model. *ACM Computer Graphics (SIGGRAPH '92)*, 26(2):253–254, July 1992.
- [14] J. T. Kajiya. Anisotropic Reflection Models. *ACM Computer Graphics (SIGGRAPH '85)*, 19(3):15–21, July 1985.
- [15] R. W. P. King and T. T. Wu. *The Scattering and Diffraction of Waves. Harvard Monographs in Applied Science. Number 7.* Harvard University Press, 1956.
- [16] W. Krueger. Intensity Fluctuations and Natural Texturing. *ACM Computer Graphics (SIGGRAPH '88)*, 22(4):213–220, August 1988.
- [17] S. G. Lipson, H. Lipson, and D. S. Tannhauser. *Optical Physics. Third Edition.* Cambridge University Press, Cambridge, England, 1995.
- [18] H. P. Moravec. 3-D Graphics and the Wave Theory. *ACM Computer Graphics (SIGGRAPH '81)*, 15(3):289–296, August 1981.
- [19] E. Nakamae, K. Kaneda, and T. Nishita. A Lighting Model Aiming at Drive Simulators. *ACM Computer Graphics (SIGGRAPH '90)*, 24(4):395–404, August 1990.
- [20] S. K. Nayar, K. Ikeuchi, and T. Kanade. Surface Reflection: Physical and Geometrical Perspectives. *IEEE Transactions on Pattern Analysis and Machine Intelligence*, 13(7):611–634, July 1991.
- [21] J. A. Ogilvy. *Theory of Scattering from Random Rough Surfaces.* Adam Hilger, Bristol, U.K., 1991.
- [22] Tomohiro Ohira. A Shading Model for Anisotropic Reflection. *Technical Report of The Institute of Electronic and Communication Engineers of Japan*, 82(235):47–54, 1983.
- [23] A. Papoulis. *Probability, Random Variables, and Stochastic Processes.* McGraw-Hill, Systems Science Series, New York, 1965.
- [24] P. Poulin and A. Fournier. A Model for Anisotropic Reflection. *ACM Computer Graphics (SIGGRAPH '90)*, 24(4):273–282, August 1990.
- [25] M. I. Sancer. Shadow Corrected Electromagnetic Scattering from Randomly Rough Surfaces. *IEEE Transactions on Antennas and Propagation*, AP-17(5):577–585, September 1969.

- [26] C. J. R. Sheppard. Imaging of random surfaces and inverse scattering in the kirchhoff approximation. *Waves in Random Media*, 8:53–66, 1998.
- [27] R. Siegel and J. R. Howell. *Thermal Radiation Heat Transfer*. Hemisphere Publishing Corp., Washington DC, 1981.
- [28] B. E. Smits and G. W. Meyer. Newton’s colors: Simulating interference phenomena in realistic image synthesis. *Proceedings of the Eurographics Workshop on Photosimulation, Realism and Physics in Computer Graphics*, pages 185–194, 1990.
- [29] J. Stam. Stochastic Rendering of Density Fields. In *Proceedings of Graphics Interface ‘94*, pages 51–58, Banff, Alberta, May 1994.
- [30] D. C. Tannenbaum, P. Tannenbaum, and M. J. Wozny. Polarization and Birefringency Considerations in Rendering. In *Computer Graphics Proceedings, Annual Conference Series, 1994*, pages 221–222, July 1994.
- [31] K. Tomiyasu. Relationship Between and Measurement of Differential Scattering Coefficient ($d\sigma/d\Omega$) and Bidirectional Reflectance Distribution Function (BRDF). *SPIE Proceedings. Wave Propagation and Scattering in Varied Media*, 927:43–46, 1988.
- [32] G. J. Ward. Measuring and Modelling Anisotropic Reflection. *ACM Computer Graphics (SIGGRAPH’92)*, 26(2):265–272, July 1992.
- [33] E. Wolf. Coherence and Radiometry. *Journal of the Optical Society of America*, 68(1), January 1978.
- [34] A. H. Zemanian. *Distribution Theory and Transform Analysis: An Introduction to Generalized Functions, with Applications*. Dover, New York, 1987.

A A Shadowing Function

The shadowing function used in He’s model applies only to isotropic surfaces. For this reason we have used a different model derived by Sancer [25]. The shadowing function is valid for a Gaussian random surface having a correlation function $C(r)$ and standard deviation σ :

$$S(\mathbf{r}) = \frac{1}{2} \left[1 + \frac{C(r)}{\sigma^2} \right] \quad (A.1)$$

where

$$C(r) = \frac{1}{2\pi} \int_0^\infty \frac{J_0(kr)}{k} dk \quad (A.2)$$

where J_0 is the Bessel function of the first kind. Since the derivatives of the correlation function depend on the correlation lengths λ_x and λ_y , this clearly shows that this shadowing function takes into account the anisotropy of the surface.

B Computing Infinite Sums

The following piece of code will compute the distribution of reflected light from the surface:

```
compute_D ( lambda, u, v, w, sigma_h, Tx, Ty )
  k = 2*PI/lambda;
  g = k*sigma_h*w; g *= g;
  if ( g > 10 ) return D_geom(u,v,w,sigma_h/Tx,sigma_h/Ty);
  tmp=1; sum=log_g=0;
  for ( m=1 ; abs(tmp)>EPS || m<3*g ; m++ ) {
    log_g += log(g/m); tmp = exp(log_g-g);
    sum += tmp*D(m,k*u,k*v,Tx,Ty);
  }
  return ( lambda*lambda*sum );
```

The function $D()$ is any one of the functions of Equation 15. This routine is a stable implementation of the infinite sum appearing in Equation 16. A naive implementation of the sum results in numerical overflows. The condition “ $m < 3 \cdot g$ ” is there to make sure that we do not exit the loop too early. This is an heuristic which has worked well in practice.

C Fourier Analysis

In this appendix we provide the main definitions and results from Fourier analysis required in this paper. Although this material is known to most researchers in computer graphics, we have included it since the steps in our derivation depend on a particular choice of the transform. Let f be a complex valued function defined over the entire plane. By function here we actually mean a generalized function or distribution since Fourier analysis has been extended to both [34]. In particular, this will allow us to state many results without having to worry about problems of convergence. A well known example of a generalized function is the two-dimensional delta function δ , which is zero everywhere except at the origin and which integrates to unity. The two-dimensional Fourier transform of the function f is defined by

$$F(\mathbf{u}, \mathbf{v}) = \int_{\mathbb{R}^2} f(\mathbf{x}) e^{-i(\mathbf{u} \cdot \mathbf{x} + \mathbf{v} \cdot \mathbf{y})} d\mathbf{x} d\mathbf{y}.$$

In general we will denote the Fourier transform of a function by the corresponding uppercase roman literal. Conversely, the inverse transform of a function F is defined by

$$f(\mathbf{x}, \mathbf{y}) = \frac{1}{(2\pi)^2} \int_{\mathbb{R}^2} F(\mathbf{u}, \mathbf{v}) e^{i(\mathbf{u} \cdot \mathbf{x} + \mathbf{v} \cdot \mathbf{y})} d\mathbf{u} d\mathbf{v}.$$

The transform and its inverse when composed reduce to the identity transformation:

$$F(\mathbf{u}, \mathbf{v}) = \int_{\mathbb{R}^2} f(\mathbf{x}, \mathbf{y}) e^{-i(\mathbf{u} \cdot \mathbf{x} + \mathbf{v} \cdot \mathbf{y})} d\mathbf{x} d\mathbf{y} \quad \text{and} \quad f(\mathbf{x}, \mathbf{y}) = \frac{1}{(2\pi)^2} \int_{\mathbb{R}^2} F(\mathbf{u}, \mathbf{v}) e^{i(\mathbf{u} \cdot \mathbf{x} + \mathbf{v} \cdot \mathbf{y})} d\mathbf{u} d\mathbf{v}.$$

Obviously the Fourier transform and its inverse are linear operators between function spaces. Let ∂_x and ∂_y denote the partial differentiation with respect to the x and the y variable respectively. Then

$$\partial_x f(\mathbf{x}, \mathbf{y}) = -i u F(\mathbf{u}, \mathbf{v}) \quad \text{and} \quad \partial_y f(\mathbf{x}, \mathbf{y}) = -i v F(\mathbf{u}, \mathbf{v}). \quad (27)$$

In other words, differentiation becomes a simple multiplication in the Fourier domain. Another property required is that the Fourier transform of the constant function $\mathbb{1}$ is equal to the delta function multiplied by \mathbb{L} . Conversely the Fourier transform of the delta function is equal to the constant function $\mathbb{1}$:

$$\mathbb{L}^{-1} \mathbb{F}\{\mathbb{1}\} = \mathbb{F}\{\delta(x)\} = \mathbb{1} = \mathbb{L} \mathbb{F}\{\delta(x)\}. \quad (28)$$

The Fourier transform of a complex vector valued function

$$\mathbb{F}\{f(x)\} = \|\mathbb{F}\{f_1(x)\}, \dots, \mathbb{F}\{f_N(x)\}\|$$

is the vector of the Fourier transforms applied to each component:

$$\mathbb{F}\{f(x)\} = \mathbb{L}^{-1} \mathbb{F}\{\mathbb{L} f(x)\} = \mathbb{L}^{-1} \mathbb{F}\{\mathbb{L} f_1(x), \dots, \mathbb{L} f_N(x)\}.$$

Finally we mention that if the function has the physical units of \mathbb{M} , then its Fourier transform has units of $\mathbb{M} \mathbb{L}^{-1}$, where \mathbb{L} is the unit of distance (meters).

D Random Functions

Here we provide a short introduction to the theory of random functions. This theory is crucial to our model since both the surface and the waves scattered from it are random functions. The theory of random functions is a vast subject, and we refer the reader to other sources for a more comprehensive study, e.g., [23]. Before presenting the main results for random functions, it is helpful to briefly introduce the concept of a random variable and state some key results that are employed in the paper.

D.1 Random Variables

A complex random variable \mathbb{X} is a function from a probability space into the complex numbers. For each event ω in the probability space, there corresponds a complex value $\mathbb{X}(\omega)$. Although the values of the variable are random, they are characterized by a probability density function $\mathbb{P}(\mathbb{X})$, i.e., some values are more likely than others. This density allows us to compute the average value of any (deterministic) function $\mathbb{F}(\mathbb{X})$ of the random variable[†]:

$$\langle \mathbb{F}(\mathbb{X}) \rangle = \int_{\mathbb{C}} \mathbb{F}(z) \mathbb{P}(z) dz,$$

where the integration is over the entire complex plane. Examples of averages are the mean $\langle \mathbb{X} \rangle$ and the variance $\langle \mathbb{X}^2 \rangle - \langle \mathbb{X} \rangle^2$ of the random variable:

$$\langle \mathbb{X} \rangle = \int_{\mathbb{C}} z \mathbb{P}(z) dz \quad \langle \mathbb{X}^2 \rangle = \int_{\mathbb{C}} z^2 \mathbb{P}(z) dz.$$

Let \mathbb{Y} be another random variable with probability density function $\mathbb{P}(\mathbb{Y})$. The distribution of both functions is then defined by the joint probability density function $\mathbb{P}(\mathbb{X}, \mathbb{Y})$. In the case of a single random variable, we can define the average value of any function $\mathbb{F}(\mathbb{X})$:

$$\langle \mathbb{F}(\mathbb{X}) \rangle = \int_{\mathbb{C}} \mathbb{F}(z) \mathbb{P}(z) dz = \int_{\mathbb{C}} \mathbb{F}(z) \mathbb{P}(z) dz.$$

[†] The case of real-valued random variables is contained in this definition by taking a distribution which is non-zero only on the real axis.

When the two variables are independent, $\rho_{12} = 0$. However, in general the two variables are dependent. One way of measuring this dependence is through the variables' correlation:

[illegible]

where “ $\bar{\cdot}$ ” denotes complex conjugation. Other important average functions of the random variables are the characteristic functions defined by

Figure 1: Schematic representation of the experimental design. The figure is divided into two main sections: 'Pretest' and 'Main Experiment'. The 'Pretest' section includes a 'Pretest' box with a 'Pretest' label and a 'Pretest' box with a 'Pretest' label. The 'Main Experiment' section includes a 'Main Experiment' box with a 'Main Experiment' label and a 'Main Experiment' box with a 'Main Experiment' label.

When the probability density functions of the random variables \mathbf{z} and \mathbf{y} are both *Gaussian* (“bell shaped”), the characteristic function have analytical expressions:

$$(29)$$

These functions play an important role in our derivation. Obviously these definitions can be generalized to any finite number of random variables. However, for our purposes these definitions suffice.

D.2 Homogeneous Random Functions

A two-dimensional random function $\mathbf{f}(\mathbf{r})$ is a mapping from the plane into the space of random variables introduced in the previous subsection. To each point $\mathbf{r} = (x, y)$ a random function associates a complex random variable $\mathbf{f}(\mathbf{r})$. For particular values of the random variables, an ordinary function is obtained which is called a *realization* of the random function. In general, the probability density functions $p(\mathbf{f}(\mathbf{r}))$ of each variable can be arbitrary. For the class of functions we are interested in here, it is sufficient to assume that each variable has the same probability density function $p(\mathbf{f}(\mathbf{r}))$. Let $\mathbf{f}(\mathbf{r}) = \mathbf{f}(x, y)$ and $\mathbf{f}(\mathbf{r}') = \mathbf{f}(x', y')$ be two random variables at different locations. As for multiple random variates, we can define the joint probability density function of the variables $\mathbf{f}(\mathbf{r})$ and $\mathbf{f}(\mathbf{r}')$. Generally, this function will depend on both the locations $\mathbf{r} = (x, y)$ and $\mathbf{r}' = (x', y')$. However, in this paper we assume that the random function is homogeneous and therefore that the joint probability density function $p(\mathbf{f}(\mathbf{r}), \mathbf{f}(\mathbf{r}'))$ depends only on the difference $\mathbf{r}'' = \mathbf{r}' - \mathbf{r} = (x' - x, y' - y)$ of the variables. Using these densities we can define ensemble averages involving functions $\mathbf{f}(\mathbf{r})$ and $\mathbf{f}(\mathbf{r}'')$:

1. **Introduction**
 2. **Background**
 3. **Methodology**
 4. **Results**
 5. **Discussion**
 6. **Conclusion**
 7. **References**
 8. **Appendix**
 9. **Figure 1**
 10. **Figure 2**
 11. **Figure 3**
 12. **Figure 4**
 13. **Figure 5**
 14. **Figure 6**
 15. **Figure 7**
 16. **Figure 8**
 17. **Figure 9**
 18. **Figure 10**
 19. **Figure 11**
 20. **Figure 12**
 21. **Figure 13**
 22. **Figure 14**
 23. **Figure 15**
 24. **Figure 16**
 25. **Figure 17**
 26. **Figure 18**
 27. **Figure 19**
 28. **Figure 20**
 29. **Figure 21**
 30. **Figure 22**
 31. **Figure 23**
 32. **Figure 24**
 33. **Figure 25**
 34. **Figure 26**
 35. **Figure 27**
 36. **Figure 28**
 37. **Figure 29**
 38. **Figure 30**
 39. **Figure 31**
 40. **Figure 32**
 41. **Figure 33**
 42. **Figure 34**
 43. **Figure 35**
 44. **Figure 36**
 45. **Figure 37**
 46. **Figure 38**
 47. **Figure 39**
 48. **Figure 40**
 49. **Figure 41**
 50. **Figure 42**
 51. **Figure 43**
 52. **Figure 44**
 53. **Figure 45**
 54. **Figure 46**
 55. **Figure 47**
 56. **Figure 48**
 57. **Figure 49**
 58. **Figure 50**
 59. **Figure 51**
 60. **Figure 52**
 61. **Figure 53**
 62. **Figure 54**
 63. **Figure 55**
 64. **Figure 56**
 65. **Figure 57**
 66. **Figure 58**
 67. **Figure 59**
 68. **Figure 60**
 69. **Figure 61**
 70. **Figure 62**
 71. **Figure 63**
 72. **Figure 64**
 73. **Figure 65**
 74. **Figure 66**
 75. **Figure 67**
 76. **Figure 68**
 77. **Figure 69**
 78. **Figure 70**
 79. **Figure 71**
 80. **Figure 72**
 81. **Figure 73**
 82. **Figure 74**
 83. **Figure 75**
 84. **Figure 76**
 85. **Figure 77**
 86. **Figure 78**
 87. **Figure 79**
 88. **Figure 80**
 89. **Figure 81**
 90. **Figure 82**
 91. **Figure 83**
 92. **Figure 84**
 93. **Figure 85**
 94. **Figure 86**
 95. **Figure 87**
 96. **Figure 88**
 97. **Figure 89**
 98. **Figure 90**
 99. **Figure 91**
 100. **Figure 92**
 101. **Figure 93**
 102. **Figure 94**
 103. **Figure 95**
 104. **Figure 96**
 105. **Figure 97**
 106. **Figure 98**
 107. **Figure 99**
 108. **Figure 100**
 109. **Figure 101**
 110. **Figure 102**
 111. **Figure 103**
 112. **Figure 104**
 113. **Figure 105**
 114. **Figure 106**
 115. **Figure 107**
 116. **Figure 108**
 117. **Figure 109**
 118. **Figure 110**
 119. **Figure 111**
 120. **Figure 112**
 121. **Figure 113**
 122. **Figure 114**
 123. **Figure 115**
 124. **Figure 116**
 125. **Figure 117**
 126. **Figure 118**
 127. **Figure 119**
 128. **Figure 120**
 129. **Figure 121**
 130. **Figure 122**
 131. **Figure 123**
 132. **Figure 124**
 133. **Figure 125**
 134. **Figure 126**
 135. **Figure 127**
 136. **Figure 128**
 137. **Figure 129**
 138. **Figure 130**
 139. **Figure 131**
 140. **Figure 132**
 141. **Figure 133**
 142. **Figure 134**
 143. **Figure 135**
 144. **Figure 136**
 145. **Figure 137**
 146. **Figure 138**
 147. **Figure 139**
 148. **Figure 140**
 149. **Figure 141**
 150. **Figure 142**
 151. **Figure 143**
 152. **Figure 144**
 153. **Figure 145**
 154. **Figure 146**
 155. **Figure 147**
 156. **Figure 148**
 157. **Figure 149**
 158. **Figure 150**
 159. **Figure 151**
 160. **Figure 152**
 161. **Figure 153**
 162. **Figure 154**
 163. **Figure 155**
 164. **Figure 156**
 165. **Figure 157**
 166. **Figure 158**
 167. **Figure 159**
 168. **Figure 160**
 169. **Figure 161**
 170. **Figure 162**
 171. **Figure 163**
 172. **Figure 164**
 173. **Figure 165**
 174. **Figure 166**
 175. **Figure 167**
 176. **Figure 168**
 177. **Figure 169**
 178. **Figure 170**
 179. **Figure 171**
 180. **Figure 172**
 181. **Figure 173**
 182. **Figure 174**
 183. **Figure 175**
 184. **Figure 176**
 185. **Figure 177**
 186. **Figure 178**
 187. **Figure 179**
 188. **Figure 180**
 189. **Figure 181**
 190. **Figure 182**
 191. **Figure 183**
 192. **Figure 184**
 193. **Figure 185**
 194. **Figure 186**
 195. **Figure 187**
 196. **Figure 188**
 197. **Figure 189**
 198. **Figure 190**
 199. **Figure 191**
 200. **Figure 192**
 201. **Figure 193**
 202. **Figure 194**
 203. **Figure 195**
 204. **Figure 196**
 205. **Figure 197**
 206. **Figure 198**
 207. **Figure 199**
 208. **Figure 200**
 209. **Figure 201**
 210. **Figure 202**
 211. **Figure 203**
 212. **Figure 204**
 213. **Figure 205**
 214. **Figure 206**
 215. **Figure 207**
 216. **Figure 208**
 217. **Figure 209**

In the remainder of this appendix and in the rest of the paper, the dependence of the average on the probability density will be dropped. Which average applies where should be obvious from the context. With these averages we can define the mean, variance and correlation of a random function as follows:

1. **General Information:**
 a. **Project Name:** [Project Name]
 b. **Client:** [Client Name]
 c. **Project Manager:** [Project Manager Name]
 d. **Project Start Date:** [Project Start Date]
 e. **Project End Date:** [Project End Date]

2. **Project Objectives:**
 a. [Objective 1]
 b. [Objective 2]
 c. [Objective 3]

3. **Project Scope:**
 a. [Scope Item 1]
 b. [Scope Item 2]
 c. [Scope Item 3]

4. **Project Budget:**
 a. **Total Budget:** [Total Budget]
 b. **Allocated Budget:** [Allocated Budget]
 c. **Remaining Budget:** [Remaining Budget]

5. **Project Risks:**
 a. [Risk 1]
 b. [Risk 2]
 c. [Risk 3]

6. **Project Deliverables:**
 a. [Deliverable 1]
 b. [Deliverable 2]
 c. [Deliverable 3]

7. **Project Status:**
 a. [Status 1]
 b. [Status 2]
 c. [Status 3]

8. **Project Notes:**
 a. [Note 1]
 b. [Note 2]
 c. [Note 3]

9. **Project Sign-off:**
 a. **Project Manager:** [Signature]
 b. **Client:** [Signature]

10. **Project Approval:**
 a. **Approval:** [Approval]
 b. **Approval Date:** [Approval Date]

respectively.

Homogeneous random functions have the property that their correlation function has a spectral representation:

$$R_X(\tau) = \int_{-\infty}^{\infty} e^{i\omega\tau} S_X(\omega) d\omega, \quad (1)$$

where $S_X(\omega)$ is a positive function called the *spectral density* of the random function. Conversely, the spectral density is a Fourier transform of the correlation function.

$$S_X(\omega) = \frac{1}{2\pi} \int_{-\infty}^{\infty} R_X(\tau) e^{-i\omega\tau} d\tau. \quad (2)$$

This is a famous result in the theory of random processes, known as the *Wiener-Khinchin theorem*.

Figure 8: Effect of some of the parameters.

(a)

(b)

(c)

(d)

Figure 9: More pictures.